Wave Breaking and Mixing at the Subtropical Tropopause

R. K. SCOTT AND J.-P. CAMMAS

Laboratoire d'Aérologie, Observatoire Midi Pyrénées, Toulouse, France

(Manuscript received 21 June 2001, in final form 15 February 2002)

ABSTRACT

This paper discusses Rossby wave breaking on the isentropic surfaces that intersect the subtropical tropopause, using winds and isentropic potential vorticity from high-resolution meteorological analysis. The focus is both on particular aspects of individual wave breaking events, as well as on more general aspects such as the spatial and temporal distribution of the mixing associated with these events.

The direction and intensity of wave breaking is shown to exhibit the same dependence on stagnation points in the wind field as that seen in previous highly idealized numerical model studies. Wave breaking that results in stratospheric intrusions into the troposphere can be categorized as weak or strong, depending on the development of filaments or larger, coherent vortices or cutoff lows. The events presented show a deep vertical structure that approximately spans the region between the 330-K and 370-K isentropic surfaces, where the tropopause is steeply sloping through the subtropical jets. This is in contrast with tropospheric intrusions into the stratosphere, which appear to be less directly related to wave breaking than to the interaction of coherent structures in the tropospheric circulation. Transport estimates during weak wave breaking are shown to be very sensitive to the definition of the tropopause.

Contour stretching is used as a measure of the mixing properties at the tropopause associated with the Rossby wave breaking and reveals longitudinal inhomogeneities that are consistent with the different structure of the subtropical jets over the Atlantic and Pacific Oceans. A strong seasonal cycle and interannual variability are also present, with generally stronger mixing in the summer and weaker mixing over the western Pacific during the warm phase of the El Niño–Southern Oscillation.

1. Introduction

The upper troposphere and lower stratosphere are characterized by marked differences in ozone concentrations and humidity, with high humidity and low ozone values in the troposphere and the reverse in the stratosphere. The strong gradients of these chemical species at the tropopause separating the two regions are indicative of a barrier to the transport of air from one region to the other. Since these two chemical species play an important role in determining the radiative properties of the two regions, it is important to develop a thorough understanding of the mechanisms by which air can cross this barrier. In this paper we consider some aspects of one such mechanism, Rossby wave breaking at the subtropical tropopause.

Rossby wave breaking is typically characterized by the irreversible deformation of potential vorticity (PV) contours on isentropic surfaces, and the subsequent mixing of different air masses. The process is found in various atmospheric contexts, such as on the edge of the stratospheric polar vortex (e.g., McIntyre and Palmer 1983; Juckes and McIntyre 1987; Norton 1994), on the low-latitude edge of the stratospheric surf zone (e.g., Polvani et al. 1995), and at the tropopause (e.g., Appenzeller et al. 1996; Peters and Waugh 1996), as well as in more idealized model settings (e.g., Polvani and Plumb 1992; Nakamura and Plumb 1994; Swanson et al. 1997). In all cases Rossby wave breaking is associated with the presence of a critical level, where the wave becomes stationary with respect to the flow field. Such critical levels are often present in the weak winds in the low-latitude lowermost stratosphere, as well as equatorward of the subtropical jets near the tropopause. When wave breaking occurs near the tropopause, stratospheric and tropospheric air may mix quasi-horizontally on those ''middleworld'' isentropic surfaces that intersect the tropopause in the wave breaking region (e.g., Holton et al. 1995).

As described in Kiladis (1998), Rossby waves propagating into low latitudes often have a typically barotropic structure. In addition, the dynamical tropopause slopes strongly upwards into the low latitudes in the region of the subtropical jet. In the light of this structure, and the associated quasi-horizontal nature of wave breaking, the principle diagnostic we use in this study is the PV on middleworld isentropic surfaces that in-

Corresponding author address: Dr. Richard K. Scott, Department of Applied Physics and Applied Mathematics, Columbia University, 200 Seeley W. Mudd Building, 500 W. 120th Street, New York, NY 10027.
E-mail: scott@appmath.columbia.edu

tersect the subtropical tropopause. On these surfaces critical levels appear as regions of weak winds relative to the phase speeds of the waves. The barotropic structure and generally deep vertical extent of the wave breaking and the subtropical tropopause region separate this type of mechanism from deformations of the more horizontally oriented midlatitude tropopause, which include tropopause folding events of the type more traditionally studied in the context of stratosphere–troposphere exchange (STE; e.g., Keyser and Shapiro 1986; Appenzeller et al. 1996). In such midlatitude tropopause folding, the ageostrophic circulation associated with jet diffluence or curvature in the presence of large wave amplitudes leads to strong baroclinicity and stratospheric air that ''descends'' along the inclined isentropic surfaces into the troposphere. On the other hand, the isentropic motion and tropopause deformations associated with Rossby wave breaking in the subtropics are quasi-horizontal, often with a deep vertical structure associated with the more vertically oriented tropopause in the jet region.

A recent climatology by Postel and Hitchman (1999) considered Rossby wave breaking on the 350-K isentropic surface, using an objective gradient reversal method to estimate the frequency and distribution of breaking events in NCEP meteorological analyses. Their study revealed a strong seasonal cycle in which wave breaking occurs predominantly in the summer (northern and southern) hemispheres, east of the outflow of the main monsoon regions. In a separate study, Waugh and Polvani (2000) considered wave breaking events that resulted in intrusions of stratospheric air deep into the tropical troposphere, these events having the largest impact on tropical tropospheric ozone heating as well as a possible influence on deep convection. Their study suggested a correspondence between the frequency of such wave breaking events and the longitudinal variations in the mean flow associated with equatorial westerly ducts over the Atlantic and Pacific Oceans. As waves propagate eastward along the subtropical jet and enter the weak westerlies east of the ducts they are meridionally extended and longitudinally compressed, leading to wave breaking and deep intrusions of stratospheric air into the tropical troposphere. In a 20-yr climatology they found that wave breaking deep into the Tropics was most frequent during Northern Hemisphere winter and during years in which the El Niño–Southern Oscillation (ENSO) was in its cold phase (La Niña). Shapiro et al. (2001) found a strong relationship between the relative frequency of LC1- and LC2-type breaking events (Thorncroft et al. 1993) between warm and cold phases of a single ENSO cycle and attributed the pattern to differences in the shear of the subtropical jets. Thus the lack of wave breaking deep into the Tropics during El Niño years found by Waugh and Polvani might also be due in part to the preference for LC2-type events during these years, and the attendant poleward propagation of wave activity.

The approach of the present study is as follows. First, we present the evolution of some individual wave breaking events at the subtropical tropopause that illustrate the structure of the wave breaking and the influence of the background wind field. These examples include wave breaking of both weak and strong intensity, and we also discuss the conditions necessary for transport of air, either from the stratosphere to troposphere, or the reverse. Second, we present a simple diagnostic of wave breaking activity that illustrates the vertical, longitudinal, seasonal and interannual variation of the mixing of stratospheric and tropospheric air by wave breaking.

The individual wave breaking events that have been selected are representative of typical atmospheric events but at the same time are sufficiently ''clean'' examples to consider the wave breaking in relative isolation from other effects. Our approach is intermediate between comprehensive case studies of complicated atmospheric processes (e.g., Appenzeller et al. 1996; Bithell et al. 1999) and conceptual, idealized models of wave breaking. Contour advection is used to show the finescale evolution of the wave breaking. We illustrate how the relation of wave breaking intensity to the background velocity field, previously seen in idealized barotropic contour models (Polvani and Plumb 1992; Nakamura and Plumb 1994; Swanson et al. 1997), is also present in real atmospheric flows. Such behavior includes the dependence of wave breaking intensity on the location of stagnation points (which take the place of critical layers when considering the breaking of a single wave crest; e.g., Polvani and Plumb 1992), and the dependence of wave breaking direction on the symmetry of the background flow (Nakamura and Plumb 1994; Peters and Waugh 1996). In particular, we find wave breaking in both directions: stratospheric air being drawn into the troposphere, and the reverse. In addition, we consider the vertical structure of the wave breaking, which shows deep filaments that appear first on the lower isentropic surfaces, below the level of the jet maximum. Finally, we consider the sensitivity of cross tropopause mass transport estimates to the choice of PV used for the tropopause, and how this sensitivity depends on breaking intensity.

During our search of individual breaking events, significant longitudinal inhomogeneity became apparent in the degree of stirring near the tropopause. By stirring, we mean the development of long contour lengths and correspondingly complex geometric structure, which is necessary for efficient mixing by smaller-scale three-dimensional turbulent motions and subsequent molecular diffusion. As a suitable diagnostic we use the contour stretching obtained after a few days of contour advection on various isentropic surfaces, and further consider the contour stretching restricted to each of the twelve 30° longitudinal bands covering each hemisphere. The results show significant longitudinal inhomogeneity that is dependent on both height and season,

and with generally more longitudinal inhomogeneity in the NH than the SH.

The structure of this paper is as follows. In section 2 we describe the meteorological analyses and the contour advection techniques and diagnostics used throughout the remainder of the paper. In section 3 we consider individual wave breaking events, focusing on the intensity and direction of the wave breaking, the vertical structure, and the sensitivity of transport calculations, and make a few remarks on the structure of the tropopause. In section 4 we consider the global structure of mixing near the tropopause, and focus on the longitudinal and vertical structure, interhemispheric differences and the dependence on the seasonal cycle and on ENSO phase. Conclusions are given in section 5.

2. Methods

We use the European Centre for Medium-Range Weather Forecasts (ECMWF) analyses with a spectral resolution of T106 to derive velocity and PV fields on various isentropic surfaces in the range 330–370 K. From these we select Rossby wave breaking events characterized by the irreversible deformation of the 2-pvu (potential vorticity unit) PV contour (or other suitable PV contour, where 1 pvu $= 10^{-6}\,\mathrm{m^2\,s^{-1}\,K\,kg^{-1}}$), which serves as our definition of the tropopause (e.g., Hoskins et al. 1985). The wave breaking events are selected to illustrate the main features of weak and strong wave breaking, and so we choose relatively clean, isolated events. We note, however, that the underlying morphology of more complicated wave breaking events often appears very similar to that of these examples, with either thin filamentation or the formation of cutoff lows being ubiquitous features. Having selected an event, we use contour advection to analyze the finescale evolution missing in the analyses (although we note that the analysis, especially at higher T213 resolution, often suggests the presence of very fine filamentation by broader filaments of lower PV intensity; i.e., they appear as ''smeared'' out). To obtain a clear picture, we first filter the PV field in Fourier space, retaining only the first seven zonal wavenumbers, and remove any small, closed contours, to leave a single, smoothly undulating contour separating stratospheric and tropospheric air. This contour is then advected for a number of days leading up to the wave breaking. The small scales that develop during this time result solely from the advection by the velocity fields. We note that the ability of contour advection to accurately reproduce the evolution of wave breaking events in the subtropics has been investigated recently by Scott et al. (2001), who showed quantitative agreement between advected PV and in situ, aircraft measurements of ozone. On the other hand, we do not expect the exact details (e.g., the position) of filamentation to be reproduced exactly by contour advection (see Methven and Hoskins 1999), though we do expect the general features to be robust.

To calculate the area of air transported on an isentropic surface in a typical wave breaking event, we coarse grain the PV field after the wave breaking event using Dritschel's (1989) contour surgery algorithm at incrementally increasing surgery scales (see, e.g., Waugh 1992; Waugh and Plumb 1994; Polvani et al. 1995) to remove the small scales. The difference in the area before and after coarse graining gives an indication of the transport involved during the wave breaking event. To isolate the transport arising from a particular wave breaking event, the area calculated is that of the intersection of the region enclosed by the contour with a longitude segment that contains the event. In section 3d below, the transport for representative events is calculated in this way using a number of different PV values for the tropopause.

Finally we use the amount of stretching of the advected contour as a diagnostic measure of the amount of small-scale structure, or complexity generated by the advection, and hence as a measure of the mixing properties at the tropopause. The stretching is defined as $\log[L(T)/L(0)]$ for some suitable T, where $L(t)$ is the contour length at time t. Bigger stretching means more small-scale structure, which leads to more efficient mixing by small-scale three-dimensional turbulent motions and diffusion at the molecular scale. We use the contour stretching as a longitudinally dependent measure of mixing on different isentropic surfaces, by using the contour length lying within each of the twelve 30° intervals [0°, 30°E], [30°, 60°E], . . . , [330°E, 360°]. This gives sufficient longitudinal resolution to illustrate differences in the small-scale development over continental and oceanic regions.

3. Characteristics of wave breaking

a. Synoptic picture

From a detailed study of wave breaking events in the 2-yr period 1998–99, we have selected two contrasting examples that illustrate, as cleanly as possible, different morphologies of PV evolution on isentropic surfaces. These events are clean enough to provide a link between comprehensive case studies of more complicated atmospheric events (e.g., Appenzeller et al. 1996; Bithell et al. 1999) and the predictions of the simple, single-layer models described above. They also enable an easier consideration of, for example, the vertical structure and the sensitivity of transport calculations.

Figure 1 shows the PV on the 350-K isentropic surface in the SH from ECMWF analyses for 2 days in May 1998. This month was characterized by a relatively undisturbed tropopause in the SH, especially over the Pacific, with a predominantly undular PV distribution that makes the growth and saturation of Rossby waves easier to identify in time series. Figure 1a shows relatively weak wave breaking, with a small amount of air with PV values up to −2 pvu being drawn off in a thin

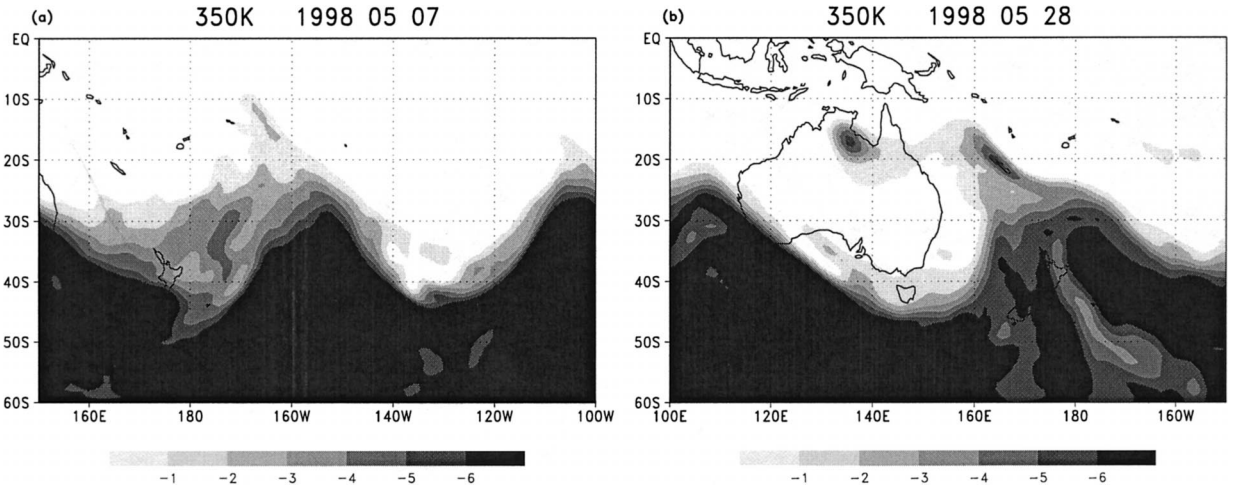

FIG. 1. PV on the 350-K isentropic surface from the ECMWF analyses on (a) 1200 UTC 7 May 1998 and (b) 1200 UTC 28 May 1998. Dark shading represents stratospheric air with absolute PV values greater than 6 pvu and the shading interval is 1 pvu.

filament up to around 10°S. Note that the analyses are unable to completely resolve this filament, but instead represent the breaking by a rather diffuse region of increased PV values. By contrast, the wave breaking shown in Fig. 1b shows a larger amount of high PV air being drawn into the tropopause. By the time indicated in the figure, what was initially a straight band of high PV air has rolled up under its own induced circulation forming a strong cutoff low situated at 18°S, 135°E.

Both of the above examples are similar in form to the upper-level evolution of LC1-type baroclinic lifecycles. At the level shown, the wave growth and ultimate breaking is associated with the second saturation phase of the ''saturation–propagation–saturation'' picture described by Thorncroft et al. (1993). The initial baroclinic growth and first saturation phase take place lower in the troposphere near the steering level where the subtropical jet is weaker.

b. Breaking intensity and small-scale evolution

We consider first how the intensity of the wave breaking depends on the location of the stagnation point, or more accurately stagnation region, in the comoving isentropic wind field. The investigation is motivated by the work of Polvani and Plumb (1992), Nakamura and Plumb (1994), and Swanson et al. (1997), who used barotropic contour dynamical models to study wave breaking in idealized vorticity distributions. These studies showed that the critical amplitude required for wave breaking is dependent on the position of a stagnation point in the comoving velocity field, that is, the velocity field relative to the phase speed of the wave. In particular, Polvani and Plumb (1992) found that wave breaking was related to the location of a stagnation point in the (comoving) velocity field as follows: no wave breaking occurred if the stagnation point was outside the vortex edge (subcritical); weak wave breaking occurred if the stagnation point was just inside the vortex edge (weakly supercritical); strong wave breaking occurred if the stagnation point was well inside the vortex edge (strongly supercritical). Chen (1996) has also shown, using a high-resolution single-layer spherical model, that wave breaking at the subtropical edge of the surf zone in the lower stratosphere depends on the zonal mean zonal velocity at 30°. Here we show that these ideas can also be applied to Rossby wave breaking events in the real atmosphere.

Figure 2 shows the time evolution and smaller scales of the weak wave breaking event of Fig. 1a using a contour advection simulation of the (SH) −2 pvu PV contour on the 350-K isentrope initialized on 5 May 1998. The evolution is characterized by the steepening of the wave crest (Fig. 2a) and the subsequent pinching off of a thin filament of stratospheric air into the troposphere (Fig. 2b). After the event the filament is stretched out further by the differential advection of the wind field and advected east. A day later, Fig. 2c, the filament is still embedded in the jet and has been advected along the jet axis, the point of attachment to the stratosphere now being located at the wave crest near 260°E, although this wave crest itself has not broken. Note that the ECMWF analyses capture the basic evolution up to around the time of Fig. 2b, but not the subsequent small-scale stretching and filamentation, this instead being represented by a diffuse region of weaker PV gradients.

In the framework of Polvani and Plumb (1992), we can describe the evolution of the wave breaking shown in Fig. 2 as weakly supercritical. Here, the ''vortex edge'' is the tropopause, or −2 pvu contour. The wind field in the frame of reference comoving with the wave (see below) is shown by the arrows in Fig. 2, and a stagnation point can be located in Fig. 2a just inside the wave crest.

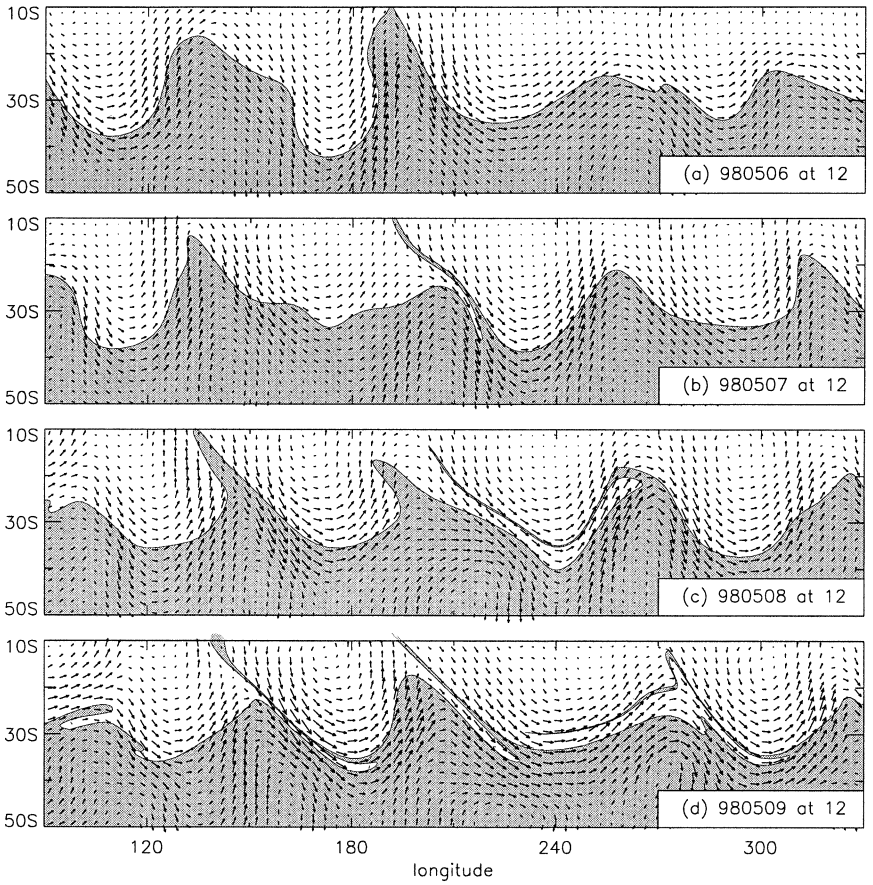

FIG. 2. PV on the 350-K isentropic surface from a contour advection simulation initialized at 1200 UTC 3 May 1998 (hereafter, 980503 at 12, etc.) prior to a weak wave breaking event near 200°E in the SH: (a) on 980506 at 12; (b) on 980507 at 12; (c) on 980508 at 12; (d) on 980509 at 12. The shaded region denotes stratospheric air with (absolute) PV values greater than 2 pvu. Arrows denote the velocity field relative to the (zonal) phase speed of the wave (estimated as 5 m s^{-1} eastward).

In contrast, Fig. 3 shows the evolution of the strong wave breaking event of Fig. 1b, a case of strongly supercritical wave breaking. Now the stagnation point, or stagnation region, is located well inside the wave crest (Fig. 3a), forming a line running down its length well into the stratosphere, and subsequently a large piece of stratospheric air is pinched off into the troposphere. The result of the wave breaking is the ejection from the stratosphere of a distinct coherent vortex patch or cutoff low (COL; Fig. 3b); this type of secondary vortex formation is characteristic of strongly supercritical wave breaking. Again, ECMWF analyses shown in Fig. 1b capture the basic evolution and formation of the secondary vortex, but not the small-scale filamentary structures linking the vortex to the tropopause or those wrapping around the COL itself (Fig. 3c). Finally, note that, although the wave has been severely diminished by the ejection of the secondary vortex, a second wave breaking event takes place immediately after the first. Again, this can be related to a stagnation point in the wind field, which is seen to persist within the crest of the wave (Figs. 3b–d).

The phase speed of the waves in each of the above cases was calculated from the phase of the zonal wavenumber-6 component (the dominant wavenumber) of the PV field, at the latitude of maximum wave amplitude (approximately 30°–35°S). This phase is plotted in Fig. 4 along with the corresponding wave amplitude for the entire month of May 1998. Both the phase and the amplitude are to a good approximation independent of height between 330 and 370 K. At the beginning of each period of wave breaking (the 6th–9th and 26th–28th) the wave-6 amplitude and phase show a marked increase to elevated values that then persist during the course of the wave breaking. In particular the phase speed appears fairly constant over each period, suggesting that critical layer arguments may be appropriate. Finally, the wave-6 amplitude is larger during the weak wave breaking than during the strong wave breaking, suggesting that it is not simply the wave amplitude that

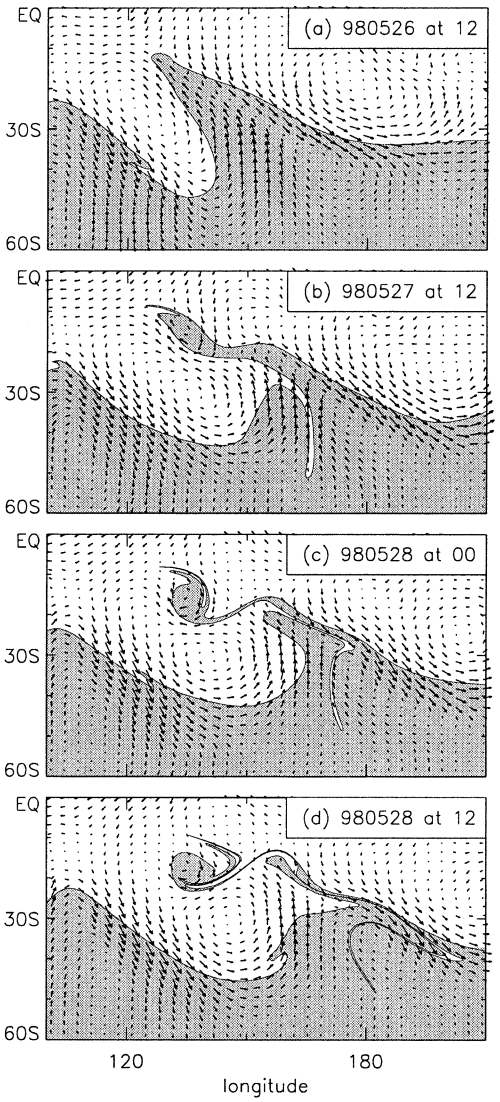

FIG. 3. As in Fig. 2, but for a contour advection simulation initialized at 1200 UTC 24 May 1998, prior to a strong wave breaking event near 180°: (a) on 980526 at 12; (b) on 980527 at 12; (c) on 980528 at 00; (d) on 980528 at 12.

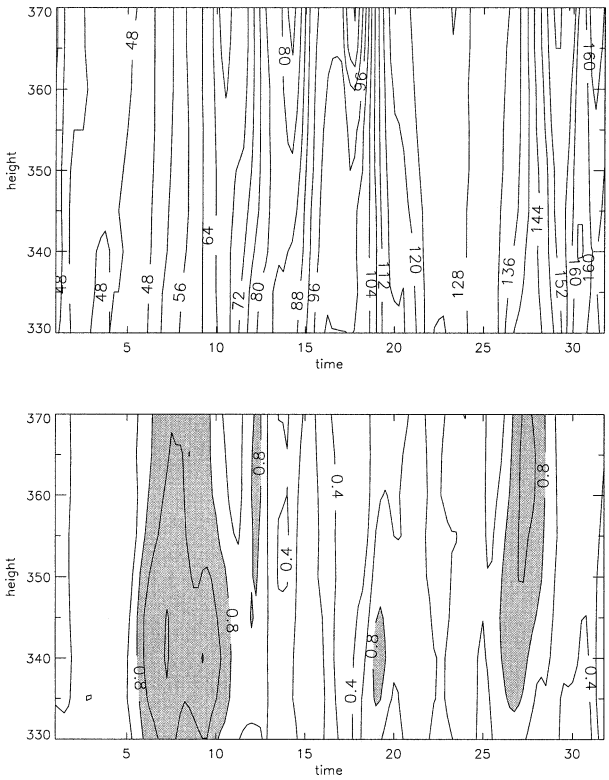

FIG. 4. (a) Phase and (b) amplitude of the zonal wavenumber-6 component of the PV at approximately 30°–35°S on 350 K for May 1998. Units in (a) are kelvins; units in (b) are pvu, and amplitudes greater than 0.8 pvu are shaded.

controls the wave breaking intensity. Consideration of the phase speed supports this, the larger phase speeds between the 26th and 28th possibly resulting in a stagnation point deeper within the stratosphere.

To assess the degree to which the background wind field predetermines the evolution of the wave breaking, contour advection calculations were made using a wind field filtered in Fourier space to contain only the first seven zonal wavenumbers. The filtering had very little effect on the weak wave breaking, filamentation occurring as it did when using the full wind field. On the other hand, there was a big change in the evolution of the strong wave breaking. While breaking still occurred there was no rollup of the filament and COL formation. Thus in the case of strong breaking the breaking wave itself substantially alters the surrounding flow field.

c. Direction of the wave breaking

The wave breaking found by Polvani and Plumb (1992) was uniquely outward in direction; that is, high-vorticity air was ejected or stripped off into the low-vorticity surroundings. This corresponds to the one way, stratosphere-to-troposphere breaking illustrated in Figs. 2 and 3. Using a similar kinematic framework Nakamura and Plumb (1994) considered the possibility for the particular structure of the background flow to allow wave breaking in the opposite direction, that is, with low-vorticity air intruding into high-vorticity surroundings. For wave breaking on a straight jet, they found that such inward breaking was possible, either for sufficiently large amplitude waves (which broke in both directions), or for weak waves provided that the critical region was on the high-vorticity side of the wave contour.

Symmetric wave breaking on a single PV contour at the tropopause, that is, both equatorward and poleward wave breaking, also occurs but is relatively rare. However, symmetric wave breaking involving more than a single PV contour occurs more frequently, an example being shown in Fig. 1a. Consideration of the wind fields

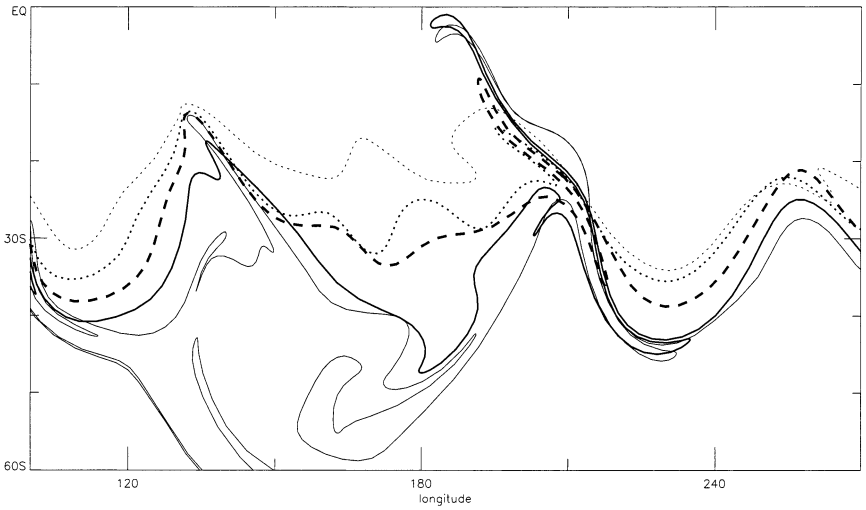

FIG. 5. Vertical structure of the weak wave breaking event on 980507 at 12 from contour advection simulations initialized on 980503 at 12, on the isentropic surfaces 370 K (thin dotted), 360 K (thick dotted), 350 K (thick dashed), 340 K (thick solid), to 330 K (thin solid). The PV contour is 2 pvu at and below 350 K, and 3 pvu above.

of this and other such events showed that there are stagnation points on both the equatorward and poleward flanks of the jet. In all cases the stagnation points are located close to the defining PV contour, and at the onset of breaking lie inside the stratosphere on the equatorward sections and inside the troposphere on the poleward sections, consistent with the kinematic ideas and the idealized model results. The poleward section of the wave breaking resembles somewhat the P1 type of poleward breaking discussed in Peters and Waugh (1996), except that in these cases where the wave breaking is symmetrical it is also, in general, much weaker than the P1-type breaking shown in that study.

Another type of inward (troposphere to stratosphere) wave breaking, resembling the P2 type of wave breaking described in Peters and Waugh (1996) was found to be more common than that arising from symmetric wave breaking. These events were characterized by strong intrusions of tropospheric air deep into the stratosphere, to as far poleward as 60° latitude. In these cases, although there are also stagnation points in the regions of the intrusions, the evolution appears to be determined instead by strong diffluence upstream and the influence of large-scale coherent structures in the troposphere, and so critical layer ideas are less relevant.

d. Vertical structure

The vertical structure of the weak and strong breaking events described in sections 3a,b are shown in Figs. 5 and 6, using an appropriate PV contour on the isentropic surfaces between 330 and 370 K. In the weak case (Fig. 5), we see that the wave breaking is a relatively deep event, with evidence of filamentation of stratospheric air on all levels, this being most pronounced at 350 K and below. Further, we see that the evolution on the lower isentropic surfaces is more developed than that higher up: the filaments are both longer and the point of attachment to the tropopause has been advected further east. This is because the wave breaks earlier at lower levels: at 330 and 340 K it breaks around 12 h earlier than at 350 K, and around 24 h earlier than at 360 K. Thus, in a three-dimensional view, the wave breaking resembles a sheet of stratospheric air being stripped off into the troposphere, with the filamentation beginning first on lower surfaces and the sheet peeling off progressively higher with increasing time. Note that on 330 K there is also a significant poleward component of the wave breaking. This can be attributed to the weaker jet at this level, resulting in the critical points on each flank of the jet lying closer to the jet axis where they can move more readily within the PV contour.

In the strong case (Fig. 6) we again see that the wave breaking is a deep event, and the formation of the COL (secondary vortex) is evident throughout the depth of the region of interest. Similar to the weak wave breaking case, the evolution on the lower isentropic surfaces is more developed than that higher up, in particular, in terms of the degree to which the ''umbilical cord'' connecting the COL to the stratospheric reservoir is stretched out and thinned by the background flow. The timing of the wave breaking, however, is now more uniform in height, and the difference in structure between the lower and upper evolution appears to stem rather from the details of the wave steepening. Finally, the COL itself is vertically orientated, despite the fact that the tropopause is not itself vertical between 330 and 370 K, suggesting the self-organizational capacity of the PV structure of the COL.

The more complicated PV structure on the lower is-

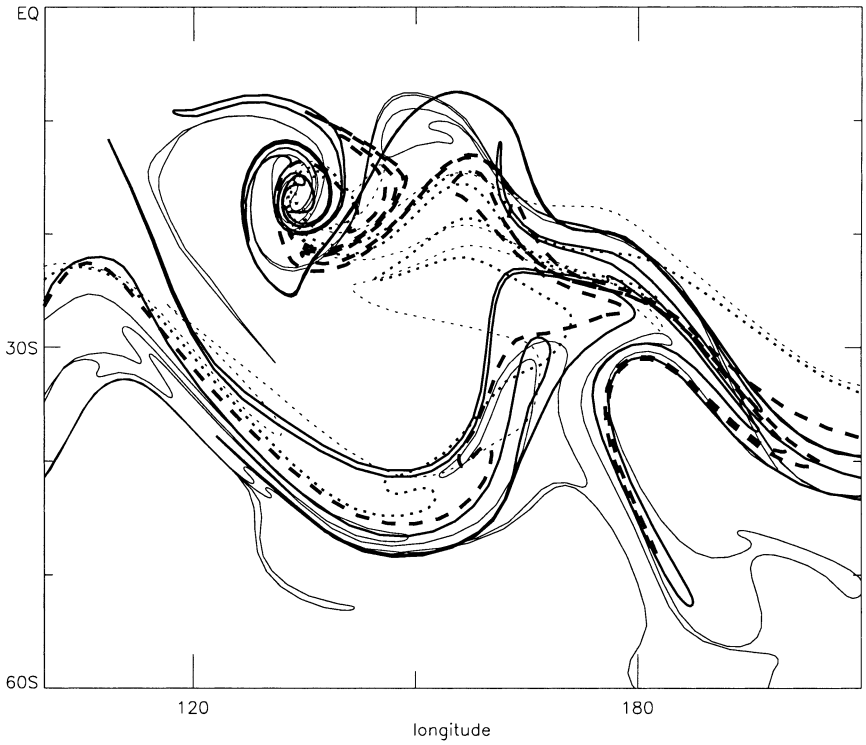

FIG. 6. As in Fig. 5, but for the strong wave breaking event on 980528 at 12 from contour advection simulations initialized on 980524 at 12.

entropic surfaces can be illustrated qualitatively by considering the contour stretching, defined as $\log[L(T)/L(0)]$ where $L(t)$ is the contour length at time t, as a function of height. Contour stretching provides a measure of the degree of isentropic mixing on each level and has been used in similar situations by, for example, Pierce and Fairlie (1993), Chen (1994), Waugh et al. (1994), and Ngan and Shepherd (1999). Here we restrict attention to the contour stretching lying in the longitudinal range (100°–270°) to isolate the height dependence of the stretching induced by the wave breaking events described above. We avoid consideration of the regions on the lower isentropic surfaces that show strong mixing that is not related to any obvious single wave breaking structure. Figure 7 shows that the contour stretching decreases with height, indicating that the strongest mixing across the tropopause occurs at lower levels. This decrease with height occurs despite the wave amplitude and phase being approximately constant with height across this region (Fig. 4), suggesting that the stronger lower-level stretching is related to the weaker lower-level winds allowing stagnation points closer to the jet axis.

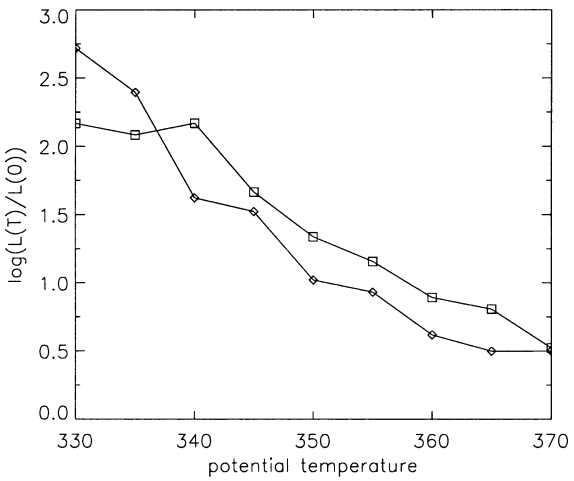

FIG. 7. Contour stretching defined as $\log[L(T)/L(0)]$ with $T = 4$ days in the longitudinal range 100°–270°E from contour advection calculations beginning on 980505 at 12 (diamonds) and on 980524 at 12 (squares) for each of the isentropic surfaces 330, 335, . . . , 370 K.

e. Mass transport

We consider next how the cross tropopause mass transport resulting from a wave breaking event depends on the intensity of the breaking. We use coarse graining to estimate the area of stratospheric air pinched off during the event. This technique has been recently applied by Dethof et al. (2000) to obtain estimates of global mass fluxes in the upper troposphere/lower stratosphere region.

Again, we consider PV contours on isentropic surfaces so that mass flux takes the form of area flux and the tropopause can be considered as a single PV contour. When there is no wave breaking and the PV contours on isentropic surfaces undulate reversibly, the material

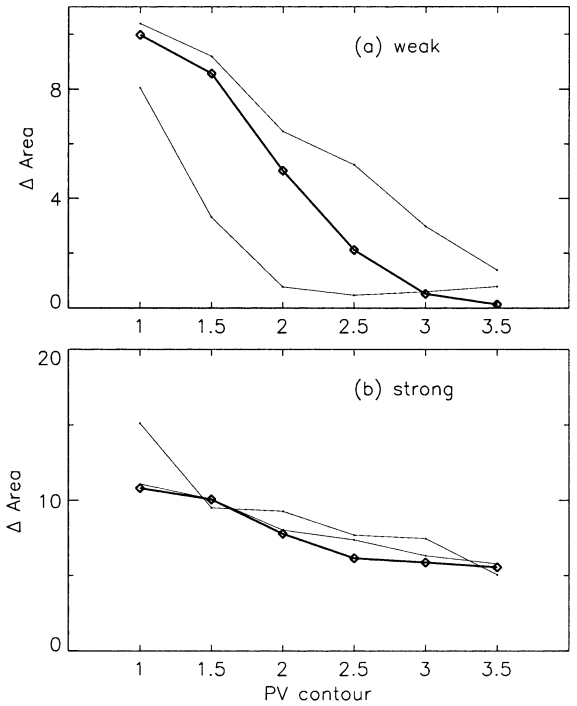

FIG. 8. Difference between contour area before and after coarse graining, as a function of the PV value used to define the contour (a) for the weak wave breaking case of Fig. 2b; (b) for the strong wave breaking case of Fig. 3c. In (b) the area difference is restricted in longitude to include only the COL. The light lines in each panel depict other weak and strong breaking examples, selected arbitrarily from the period 1998–99. Units of area are $10^{-3} \times r^2$, where r is the earth's radius.

conservation of these contours implies zero mass flux across the tropopause. For both the weak and the strong wave breaking events presented in sections 3a,b we define the transport to be the difference between the area enclosed by the contour at the time of the wave breaking and the area enclosed by the coarse-grained contour. The wave is considered (subjectively) as breaking when the PV contours cease to undulate smoothly and high PV air is pinched off the wave crest (as in Figs. 2b and 3c). We test the sensitivity of the transport to the choice of PV contour by repeating the calculation for a range of PV values between 1.0 and 3.5 pvu.

The results are shown in Fig. 8a for the weak wave breaking (diamonds) and in Fig. 8b for the strong wave breaking. Examples of a few other events are also included (light lines) for comparison. Since the intensity of the wave breaking is closely related to the area of stratospheric air pinched off into the tropopause, somewhat by definition, it is evident that the values obtained from the coarse-graining calculation will be smaller in the weak case than in the strong. What is more interesting is the different dependence on the defining PV contour between the weak and strong cases. In both cases there is a decrease in transport with increasing PV value, since higher PV contours lie closer to the stratospheric side of the tropopause region, and since each PV contour is materially conserved by the advection. However, the relative decrease is much stronger in the weak breaking case than in the strong.

The difference between the two cases can again be understood by considering the location relative to the PV tropopause of the stagnation point in the comoving velocity field. Because the PV gradients are large at the tropopause, if the stagnation point is located close to this region (relative to the width of the region), then the wave breaking intensity, and hence transport, will be very sensitive to the particular choice of PV contour. On the other hand, if the stagnation point lies further from the region of strong PV gradients (relative to the width of this region), then the distance between the stagnation point and the defining contour will be relatively insensitive to the choice of PV value. Thus we see relatively little sensitivity on the PV contour for the COL of the strong wave breaking case but considerable sensitivity in the weak case.

f. The structure of the tropopause

In the weak wave breaking event described in sections 3a,b above, the point at which the filament connects to the tropopause is advected east beyond the crest of the breaking wave. Such behavior was found to be a general feature of weak wave breaking: typically the filament resulting from a wave breaking event becomes so stretched out to small scales that it no longer has any influence on the background flow field and is simply advected away. Since the point of connection to the tropopause is typically in a region of strong westerlies, the advection at this point can be rapid relative to the phase propagation of the wave, which is determined by the baroclinic development lower down where the background velocity is smaller. On the other hand, if the extremity of the filament penetrates sufficiently deep into the weak winds in the Tropics, then advection of the extremity will be weak and the filament will undergo further stretching.

For example, for the period shown in Fig. 2, the first wave breaking occurs on 7 May near 200°E (Fig. 2b) and the resulting filament is stretched as the connection point is advected east. By 8 May (Fig. 2c), the filament is connected at the wave crest located near 270°E, giving the false impression that it is at this crest that the wave breaks. Further wave breaking at the original crest at 200° and at the crest at 140° occurs on 8 May and the resulting filaments are again advected east. By 9 May (Fig. 2d) the combination of the new wave breaking and the old filament collapsing back toward the tropopause begins to create a complex structure near the tropopause.

Complex structure near dynamical transport barriers, of which the tropopause and stratospheric polar vortex edge are examples, has been discussed previously in various contexts. Using a barotropic contour dynamical model [the same as that of Polvani and Plumb (1992)],

Koh and Plumb (2000) investigated the transport of air across a vortex edge using lobe-dynamical techniques. They found significant transport in both directions contrary to that indicated by consideration of the vortex dynamics, and interpreted this as resulting from differences in the location of the kinematic, lobe-dynamical boundary and the dynamical PV-defined boundary. K. Bowman (2001, personal communication) and Joseph and Legras (2002) used similar diagnostic tools on real velocity fields near the polar vortex edge and found two way transport across a kinematic barrier between the surf zone and a stochastic layer equatorward of the dynamical polar vortex edge. Figure 2d suggests how such a stochastic layer may be formed, with successive filamentation, stretching and collapsing back toward the tropopause. In this framework, it is incorrect to consider the totality of the filament in Fig. 2b, say, as contributing to stratospheric air mixing into the troposphere (although some of it may). Because of the collapse back onto the tropopause, it instead contributes to a stochastic or mixed layer of finite thickness near the tropopause, some of which will be mixed out into the troposphere by subsequent, possibly stronger, wave breaking.

4. Spatial and temporal distribution of mixing

Although the examples in the previous section were taken from the SH, which generally enabled the selection of cleaner breaking events, wave breaking at the subtropical tropopause is of course common to both hemispheres. In the NH, because of generally less zonally homogeneous flow, more complicated behavior often arises because of interactions between different wave breaking events. To avoid the need for explicit consideration of this complicated behavior, in this section we consider a more general diagnostic of the mixing properties at the tropopause, the stretching of the PV contour defining the tropopause. We use this diagnostic to provide a picture of the longitudinal preference of wave breaking, the variation of the mixing intensity with height, interhemispheric differences and seasonal and interannual variability. In particular, we show that there is strong longitudinal inhomogeneity in mixing strength in the NH, less inhomogeneity in the SH, and that this pattern also has considerable dependence on both the annual cycle and the ENSO phase.

a. Longitudinal preference for wave breaking

During our investigation of individual wave breaking events, a clear longitudinal preference for wave breaking emerged, most particularly on the lower isentropic surfaces in the NH. This preference was observed most easily in the complexity of the PV contour, and the associated contour length can be related to the mixing properties of the flow as described in section 3d above. An example is shown in Fig. 9, which shows the 2-pvu contour on 330 K after 4 days of a contour advection simulation. It illustrates the complex structure and significant small-scale generation in the longitudinal region 90°W–30°E, with a smoother tropopause at other longitudes.

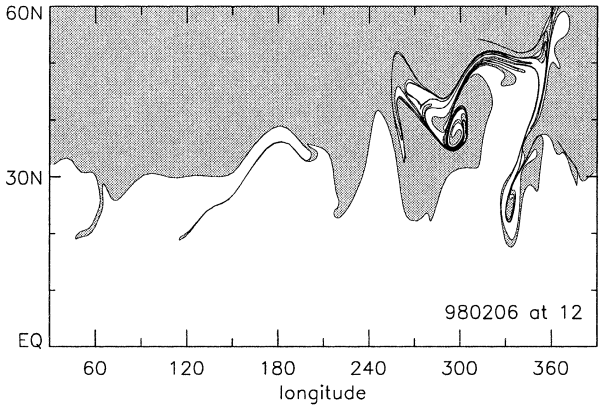

FIG. 9. PV on the 330-K isentropic surface on 980206 at 12 from a contour advection simulation initialized on 980202 at 12. The contour denotes the 2-pvu PV value.

To illustrate that the longitudinal inhomogeneity seen in Fig. 9 is a persistent feature of the tropospheric evolution, and not particular to that single mixing event, we formed a composite winter from a series of contour advection simulations. For the months of December, January, February, for each of the years 1979–99, we ran simulations beginning every second day, integrating each for 4 days on each of the isentropic surfaces 330, 350, and 370 K. From each simulation we then calculated the total contour length lying within twelve 30° longitude bands covering the globe, that is, the total contour length lying within each of the ranges 0°–30°E, 30°–60°E, . . . , 330°E–360°. The stretching is defined as $\log[L(T)/L(0)]$ where $L(t)$ is the contour length lying within each longitudinal band at time t. (Note that on 370 K it was necessary to use the 4-pvu contour as the definition of the tropopause, which was, in general, closer to the region of strong PV gradients than the 2-pvu contour.)

The resulting stretching, averaged over the winter and over all years, gives an indication of the longitudinal structure of the mixing properties of the flow, and is shown in Fig. 10a. These show a pronounced longitudinal structure on the 330-K surface, with a strongly disturbed tropopause (large stretching, implying strong mixing in the tropopause region) centered on the region 330°E–360°, that is, over the eastern Atlantic and northwest Africa, and a region of more stable tropopause (small contour length, implying weak mixing in the tropopause region) centered on the region 120°E–180°, over the western Pacific. (In each case the relevant latitude is between 25° and 35°.) A secondary maximum in stretching is visible over the eastern Pacific at 210°–270°E, which persists on the 350- and 370-K surfaces, where it dominates the distribution. Note that because of the advective nature of the stretching diagnostic, Fig. 10 gives a picture

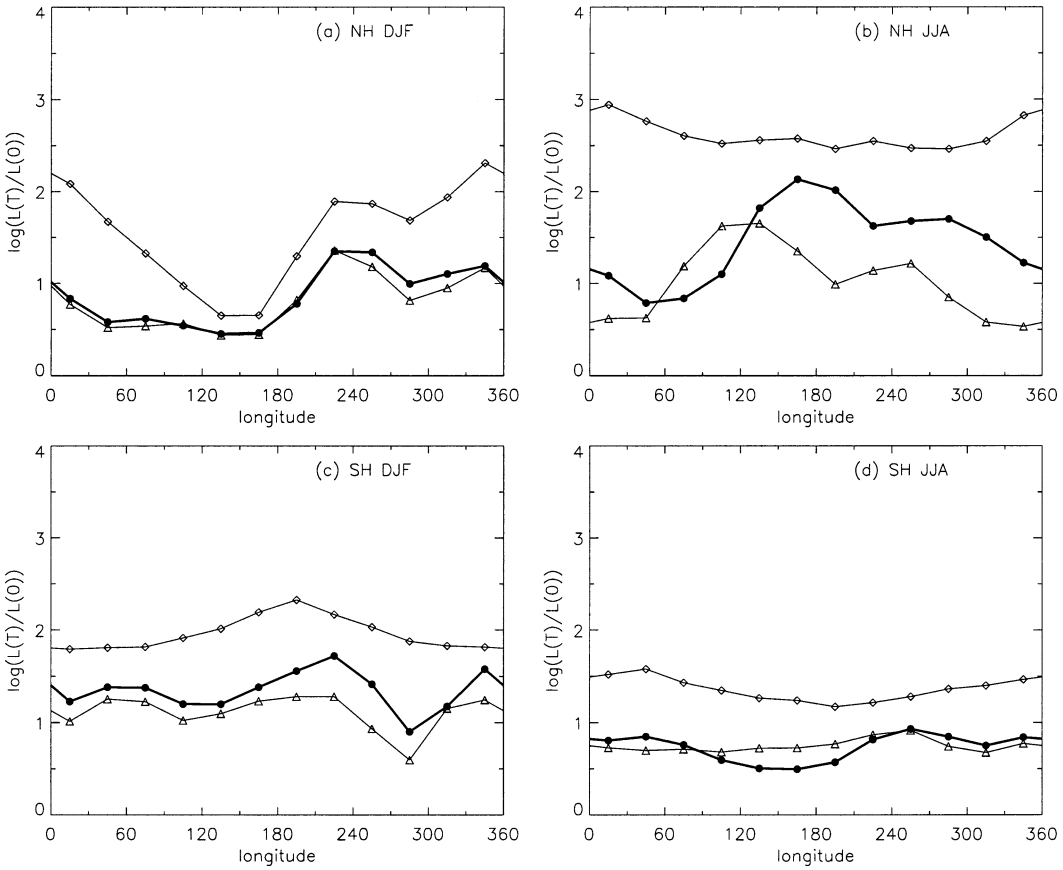

FIG. 10. Average contour stretching in each of the longitudinal ranges 0°–30°E, 30°–60°E, . . . , 330°E–360°, plotted as a function of longitude, from contour advection simulations beginning every second day during the 3-month periods Dec–Feb (DJF) and Jun–Aug (JJA) averaged over 20 yr from 1979–99: (a) NH DJF; (b) NH JJA; (c) SH DJF; (d) SH JJA. Stretching was calculated as $\log[L(T)/L(0)]$ with $T = 3$ days, where $L(t)$ is the contour length lying in a particular longitude range at time t after the beginning of the advection. The three lines represent the contour stretching on the isentropic surfaces at 330 K (diamonds), 350 K (filled circles), and 370 K (triangles).

of stretching that is skewed slightly eastward. As in section 3d above, the stretching shows there is a large vertical variation in the mixing intensity at the tropopause. In particular, over the Atlantic there is a large change in the mixing intensity somewhere between 330 and 350 K, with strong mixing at lower levels.

The weaker mixing intensity over the Pacific is associated with a strong and approximately zonal subtropical jet, as can be seen from Fig. 11a, which shows a cross section at 180° of the monthly mean zonal winds and potential temperature for January 1998. As discussed by Nakamura (1992), when the strength of the subtropical jet exceeds a critical value, as it does in winter over the Pacific, further increase in the strength of the jet results in a decrease of the baroclinic wave activity at upper levels, associated with trapping of the waves at lower levels. By contrast, Fig. 11b shows a much weaker subtropical jet over the Atlantic (at 330°E), as well as the existence of a weaker second jet centered on 45°N. The increased mixing intensity over this region is then consistent with recent work by S. Lee (2001, personal communication) that identifies this second jet as an eddy driven jet, resulting from increased baroclinicity poleward of the weak subtropical jet. Thus the stronger forcing by sea surface temperature in the western Pacific contributes to a locally stronger Hadley circulation and subtropical jet, and consequently to weaker mixing at upper levels, whereas the weaker subtropical jet over the Atlantic, together with the warm Gulf Stream results in a higher-latitude baroclinic region, a resulting eddy driven jet, and stronger mixing.

Although the winter troposphere is dynamically more active than the summer, recent studies (Postel and Hitchman 1999; Haynes and Shuckburgh 2000; Allen and Nakamura 2001) have shown that the winter tropopause is typically more stable than the summer tropopause. Different explanations are possible. One possibility is the eddy homogenization of PV: the stronger eddy activity in the winter troposphere, and hence stronger erosion of PV at the tropopause, creates stronger PV gradients at the tropopause. The stronger gradients in turn

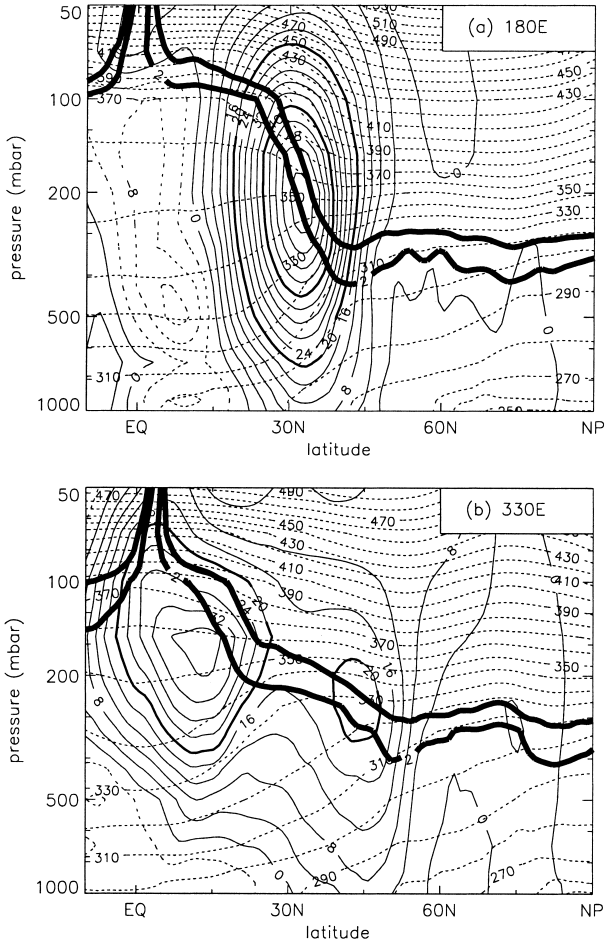

FIG. 11. Jan 1998 monthly mean meridional cross sections of zonal wind and potential temperature at (a) 180°; (b) 330°E. Solid lines denote positive zonal wind, dotted lines denote negative zonal wind and potential temperature, and the thick lines denote the monthly mean 2- and 4-pvu potential vorticity contours.

can sustain large Rossby wave amplitudes before distorting irreversibly. Another possibility is the effect of the summer monsoon circulation on the location of the tropopause (e.g., Dunkerton 1995; Dethof et al. 1999). Figure 10b shows the distribution of stretching for the NH summer, averaged over June, July, and August (1979–99), and demonstrates the generally stronger mixing intensity during the summer than that during the winter. A maximum over the western Pacific is particularly evident at 350 K, consistent with the longitudinal distribution of wave breaking found by Postel and Hitchman (1999, their Fig. 4a), who related the increase in wave breaking over this region to outflow from the Indian monsoon.

b. Interhemispheric differences

The more zonally homogeneous troposphere in the SH, resulting from smaller topography and land–sea temperature contrasts, results in a more uniformly undular tropopause, on which wave disturbances or wave breaking can develop over a greater range of longitudes. Figure 10d shows the longitudinal dependence of the contour stretching for the winter SH tropopause. Compare this with the corresponding plot for the NH winter, shown in Fig. 10a. On all isentropic surfaces the longitudinal inhomogeneity seen in the NH is much weaker, the SH distribution being almost completely flat. However, there is still a marked separation between 330 and 350 K in the mixing intensity at the tropopause, with more mixing occurring on lower levels, as in the NH. Figure 10c shows the contour stretching for the summer SH tropopause. Compare this with Fig. 10b and Fig. 10d. The structure here is again flatter than the NH summer and the overall values are higher than the SH winter. Again note that the longitudinally flat structure is comparable with that of Fig. 5a of Postel and Hitchman (1999), in particular the agreement of the location of the minimum between 270° and 300°E and the small maxima on either side.

c. Interannual variability

Recently, Waugh and Polvani (2000) have noted the dependence of Rossby wave breaking deep into the Tropics on the phase of ENSO, through its effect on the strength of the subtropical jet. In this section we separate the 20-yr climatology shown in Fig. 10, according to whether ENSO is in its warm or cold phase based on the value of the Niño-3.4 index, as shown in Fig. 12.

One effect of a warm ENSO phase on the tropospheric circulation is a stronger and more zonal subtropical jet over the Pacific. This is reflected most clearly in the mixing intensities shown in Figs. 12a–b, with slightly lower values over the NH eastern Pacific between 180° and 240°E during the warm phase than during the cold, consistent with low-level trapping of waves by stronger vertical shear. The clear maximum over the NH eastern Pacific during the cold phase is also consistent with the distribution of Rossby wave breaking on 350 K found recently by Waugh and Polvani (2000, their Fig. 2b), which showed a maximum in the NH winter, associated with equatorial westerly ducts, that had a similar dependence on ENSO phase. Another perspective on the different mixing properties during the different ENSO phases was provided recently by Shapiro et al. (2001), who showed that LC1-type baroclinic development was preferred during the cold ENSO phase, and LC2-type during the warm. The more poleward propagation of wave activity during LC2 may therefore also help explain the weaker mixing over the eastern Pacific during the warm phase compared to that in the cold.

The biggest dependence of the mixing intensity on the ENSO phase is seen at 350 and 370 K. Note in particular that the mixing intensities on these two levels appear very similar, indicating that much of the wave breaking in this region is vertically uniform. On 330 K,

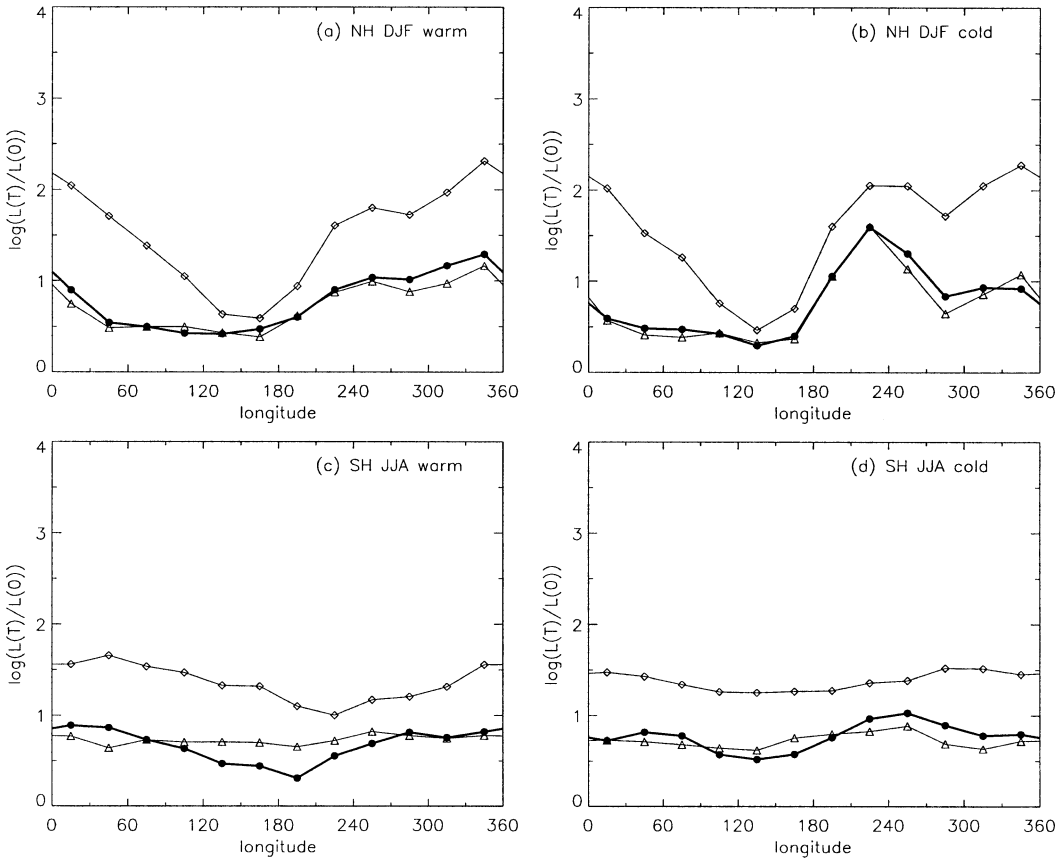

FIG. 12. Same as Figs. 10a–d, but the average taken over years in which ENSO was in the warm phase and cold phase: (a) NH DJF warm phase (1983, 1987, 1992, 1998), (b) NH DFJ cold phase (1985, 1989, 1999, 2000), (c) SH JJA warm phase (1982, 1987, 1991, 1997), and (d) SH JJA cold phase (1985, 1988, 1998, 1999).

stretching values are consistently higher than at 350 K and the ENSO signal is small. Instead, the overall longitudinal distribution seen in Fig. 10a remains, with a marked minimum in mixing intensity over the western Pacific and a strong maximum over the eastern Atlantic. As described in section 4a above, this distribution is most likely due to the different storm track characteristics arising from the stronger Pacific jet and the more poleward-extending baroclinicity over the Atlantic. Note that meridional cross sections of zonal velocity over the Atlantic during the cold ENSO phase (not shown) also show a double jet structure similar to that shown in Fig. 11b for the warm phase.

Finally, from Figs. 12c,d we see that, in the SH winter, there is very little dependence of the stretching on the ENSO phase, although the distribution on 350 K appears to have slightly more longitudinal structure during the warm phase. As mentioned previously the longitudinal structure in the SH is in general much flatter than that of the NH. Note that, as in the NH, the stretching is similar between 350 and 370 K and higher at 330 K, and the SH values are on average slightly smaller than those of the NH.

5. Conclusions

Some examples of Rossby wave breaking at the tropopause have been shown, illustrating the dependence of the isentropic potential vorticity evolution and isentropic transport upon the wave breaking intensity, and the influence of the background wind fields. The breaking intensity was shown to depend on stagnation points in the wind field, in agreement with the predictions of idealized model studies. Wave breaking was shown to occur in both directions, that is, effecting the transport of air from stratosphere to troposphere or vice versa, although weak breaking in the sense of troposphere to stratosphere was relatively rare. All cases shown possessed a deep vertical structure spanning the region between about 330 and 370 K, suggesting that these events could contribute significantly to the global stratosphere–troposphere exchange. It was shown, however, that estimates of the transport associated with individual events are rather sensitive to the definition of the tropopause, and so estimates of global transport based on estimates of individual events together with wave breaking climatologies will need to take this sensitivity into account.

In addition it was shown that the air near the tropopause is likely to have a complex structure, of mixed stratosphere/troposphere origin, and that filamentation from weak wave breaking events may act mostly to contribute to this structure rather than to the direct mixing of stratospheric air into the troposphere. Future studies using aircraft measurements in this region could reveal more quantitatively the nature of this structure, and provide guidance for the reduction of the sensitivity of transport estimates.

A 20-yr climatology showed that the general mixing properties at the subtropical tropopause, of which Rossby wave breaking appears to be the main contribution around 350 K, possess considerable spatial and temporal variability. In particular, there was strong longitudinal inhomogeneity in the NH, which also showed significant seasonal and interannual variability. On the 330-K surface in the winter NH a minimum in mixing intensity over the Pacific and a maximum over the Atlantic appeared as robust features, independent of the ENSO phase, and are probably consequences of the quasi-permanent features of the stronger subtropical jet over the Pacific and a wider baroclinic zone and secondary eddy-driven jet over the Atlantic. The NH 350- and 370-K surfaces showed nearly identical mixing characteristics, with a less pronounced winter maximum over the Atlantic, and a summer maximum over the Pacific, consistent with previous studies. On these higher isentropic surfaces the mixing intensity over the NH winter eastern Pacific was more strongly ENSO dependent, with a strong maximum in mixing intensity during the cold phase, and a suppression of mixing during the warm phase, consistent with the modification by ENSO of the subtropical jet in this region. In the SH the longitudinal distribution was in general much flatter and both hemispheres showed stronger mixing during the summer, consistent with earlier climatologies of wave breaking and mixing.

Acknowledgments. The authors wish to thank Dr. Lorenzo Polvani for prompting the investigation of the vertical structure presented in section 3d, Dr. Sukyoung Lee and Dr. Emily Shuckburgh for helpful discussion, and an anonymous referee for detailed and insightful comments that led to significant improvements of the manuscript. R. K. Scott was supported by the European Commission under Contract EVK2-1999-00015.

REFERENCES

Allen, D. R., and N. Nakamura, 2001: A seasonal climatology of effective diffusivity in the stratosphere. *J. Geophys. Res.*, **106,** 7917–7935.

Appenzeller, C., H. C. Davies, and W. A. Norton, 1996: Fragmentation of stratospheric intrusions. *J. Geophys. Res.,* **101,** 1435–1456.

Bithell, M., L. J. Gray, and B. D. Cox, 1999: A three-dimensional view of the evolution of midlatitude stratospheric intrusions. *J. Atmos. Sci.,* **56,** 637–688.

Chen, P., 1994: The permeability of the Antarctic vortex edge. *J. Geophys. Res.*, **99,** 20 563–20 571.

——, 1996: The influences of zonal flow on wave breaking and tropical–extratropical interaction in the lower stratosphere. *J. Atmos. Sci.,* **53,** 2379–2392.

Dethof, A., A. O'Neill, J. M. Slingo, and H. G. J. Smit, 1999: A mechanism for moistening the lower stratosphere involving the Asian summer monsoon. *Quart. J. Roy. Meteor. Soc.,* **125,** 1079–1106.

——, ——, and ——, 2000: Quantification of the isentropic mass transport across the dynamical tropopause. *J. Geophys. Res.,* **105,** 12 279–12 293.

Dritschel, D. G., 1989: Contour dynamics and contour surgery: Numerical algorithms for extended, high-resolution modelling of vortex dynamics in two-dimensional, inviscid, incompressible flows. *Comput. Phys. Rep.*, **10,** 78–146.

Dunkerton, T. J., 1995: Evidence of meridional motion in the summer lower stratosphere adjacent to monsoon regions. *J. Geophys. Res.,* **100,** 16 675–16 688.

Haynes, P. H., and E. F. Shuckburgh, 2000: Effective diffusivity as a diagnostic of atmospheric transport. II. Troposphere and lower stratosphere. *J. Geophys. Res.*, **105,** 22 795–22 810.

Holton, J. R., P. H. Haynes, M. E. McIntyre, A. R. Douglass, R. B. Rood, and L. Pfister, 1995: Stratosphere–troposphere exchange. *Rev. Geophys.,* **33,** 403–439.

Hoskins, B. J., M. E. McIntyre, and A. W. Robertson, 1985: On the use and significance of isentropic potential-vorticity maps. *Quart. J. Roy. Meteor. Soc.,* **111,** 877–946.

Joseph, B., and B. Legras, 2002: Relation between kinematic boundaries, stirring, and barriers for the Antarctic polar vortex. *J. Atmos. Sci.,* **59,** 1198–1212.

Juckes, M. N., and M. E. McIntyre, 1987: A high resolution, one-layer model of breaking planetary waves in the stratosphere. *Nature,* **328,** 590–596.

Keyser, D., and M. A. Shapiro, 1986: A review of the structure and dynamics of upper-level frontal zones. *Mon. Wea. Rev.,* **114,** 452–499.

Kiladis, G. N., 1998: Observations of Rossby waves linked to convections over the eastern tropical Pacific. *J. Atmos. Sci.,* **55,** 321–339.

Koh, T.-Y., and R. A. Plumb, 2000: Lobe dynamics applied to barotropic Rossby-wave breaking. *Phys. Fluids,* **12,** 1518–1528.

McIntyre, M. E., and T. N. Palmer, 1983: Breaking planetary waves in the stratosphere. *Nature,* **305,** 593–600.

Methven, J., and B. Hoskins, 1999: The advection of high-resolution tracers by low-resolution winds. *J. Atmos. Sci.,* **56,** 3262–3285.

Nakamura, H., 1992: Midwinter suppression of baroclinic wave activity in the Pacific. *J. Atmos. Sci.,* **49,** 1629–1642.

Nakamura, M., and R. A. Plumb, 1994: The effects of flow asymmetry on the direction of Rossby wave breaking. *J. Atmos. Sci.,* **51,** 2031–2045.

Ngan, K., and T. G. Shepherd, 1999: A closer look at chaotic advection in the stratosphere. Part II: Statistical diagnostics. *J. Atmos. Sci.,* **56,** 4153–4166.

Norton, W. A., 1994: Breaking Rossby waves in a model stratosphere diagnosed by a vortex-following coordinate system and a technique for advecting material contours. *J. Atmos. Sci.,* **51,** 654–673.

Peters, D., and D. W. Waugh, 1996: Influence of barotropic shear on the poleward advection of upper-tropospheric air. *J. Atmos. Sci.,* **53,** 3013–3031.

Pierce, B. R., and T. D. A. Fairlie, 1993: Chaotic advection in the stratosphere: Implications for the dispersal of chemically perturbed air from the polar vortex. *J. Geophys. Res.,* **98,** 18 589–18 595.

Polvani, L. M., and R. A. Plumb, 1992: Rossby wave breaking, microbreaking, filamentation and secondary vortex formation: The dynamics of a perturbed vortex. *J. Atmos. Sci.,* **49,** 462–476.

——, D. W. Waugh, and R. A. Plumb, 1995: On the subtropical edge of the stratospheric surf zone. *J. Atmos. Sci.*, **52,** 1288–1309.

Postel, G. A., and M. H. Hitchman, 1999: A climatology of Rossby waves breaking along the subtropical tropopause. *J. Atmos. Sci.*, **56,** 359–373.

Scott, R. K., J.-P. Cammas, P. Mascart, and C. Stolle, 2001: Stratospheric filamentation into the upper tropical troposphere. *J. Geophys. Res.*, **106,** 11 835–11 848.

Shapiro, M. A., H. Wernli, N. A. Bond, and R. Langland, 2001: The influence of the 1997–1999 ENSO on extratropical baroclinic life cycles over the eastern North Pacific. *Quart. J. Roy. Meteor. Soc.*, **127,** 331–342.

Swanson, K. L., P. J. Kushner, and I. M. Held, 1997: Dynamics of barotropic storm tracks. *J. Atmos. Sci.*, **54,** 791–810.

Thorncroft, C. D., B. J. Hoskins, and M. E. McIntyre, 1993: Two paradigms of baroclinic-wave life-cycle behaviour. *Quart. J. Roy. Meteor. Soc.*, **119,** 17–55.

Waugh, D. W., 1992: The efficiency of symmetric vortex merger. *Phys. Fluids*, **4A,** 1745–1758.

——, and R. A. Plumb, 1994: Contour advection with surgery: A technique for investigating finescale structure in tracer transport. *J. Atmos. Sci.*, **51,** 530–540.

——, and L. M. Polvani, 2000: Climatology of intrusions into the tropical upper troposphere. *Geophys. Res. Lett.*, **27,** 3857–3860.